***SPECIAL REPORT***

# WMAP: A Radiological Analysis

Pierre-Marie Robitaille

*Dept. of Radiology, The Ohio State University, 130 Means Hall, 1654 Upham Drive, Columbus, Ohio 43210, USA*

E-mail: robitaille.1@osu.edu

In this work, results obtained by the WMAP satellite are analyzed by invoking established practices for signal acquisition and processing in nuclear magnetic resonance (NMR) and magnetic resonance imaging (MRI). Dynamic range, image reconstruction, signal to noise, resolution, contrast, and reproducibility are specifically discussed. WMAP images do not meet accepted standards in medical imaging research. WMAP images are obtained by attempting to remove a galactic foreground contamination which is 1,000 times more intense than the desired signal. Unlike water suppression in biological NMR, this is accomplished without the ability to affect the signal at the source and without *a priori* knowledge. Resulting WMAP images have an exceedingly low signal to noise (maximum 1–2) and are heavily governed by data processing. Final WMAP internal linear combination (ILC) images are made from 12 section images. Each of these, in turn, is processed using a separate linear combination of data. The WMAP team extracts cosmological implications from their data, while ignoring that the ILC coefficients do not remain constant from year to year. In contrast to standard practices in medicine, difference images utilized to test reproducibility are presented at substantially reduced resolution. ILC images are not presented for year two and three. Rather, year-1 data is signal averaged in a combined 3-year data set. Proper tests of reproducibility require viewing separate yearly ILC images. Fluctuations in the WMAP images arise from the inability to remove the galactic foreground, and in the significant yearly variations in the foreground itself. Variations in the map outside the galactic plane are significant, preventing any cosmological analysis due to yearly changes. This occurs despite the masking of more than 300 image locations. It will be advanced that any "signal" observed by WMAP is the result of foreground effects, not only from our galaxy, but indeed yearly variations from every galaxy in the Universe. Contrary to published analysis, the argument suggests there are only questionable findings in the anisotropy images, other than those related to image processing, yearly galactic variability, and point sources. Concerns are also raised relative to the validity of assigning brightness temperatures in this setting.

## 1 Introduction

The WMAP satellite [1] was launched with the intent of measuring the microwave signals present in space. It is widely held that these signals are anisotropic and relay information relative to the creation and formation of the early Universe [1–27]. WMAP has been hailed as providing some of the most important findings in science [2]. Reports by Spergel et. al. [15] and Bennett et. al. [7] are highly cited [28]. The ensemble of WMAP publications [3–26] appears to constitute a phenomenal assortment of data. WMAP is being praised both for its precision and the insight it provides into the earliest stages of the formation of the Universe [1, 2]. NASA and the WMAP team of scientists, representing the premier academic institutions [1], have made numerous claims, most notably stating that their data enables them to visualize what happened in the first trillionth of a second after the Big Bang [27]. From data with a signal to noise just beyond 1, a number of constants is provided relative to the age of the Universe ($13.7\pm0.2$ Gyr), the amount of dark energy ($\sim$73%), dark matter ($\sim$22%), and baryons density or "real" matter ($\sim$4%) [7, 25]. It is surmised that "decoupling" occurred just after the Big Bang ($379\pm8$ kyr) at a redshift of $1089\pm1$. The thickness of the decoupling surface is given as $195\pm2$, and the total mass-energy in the Universe ($1.02\pm0.02$) is also amongst the constants [7, 25].

WMAP does not measure the absolute intensity of any given microwave signal. Rather, it is equipped with antennae whose difference is constantly recorded. Thus, all WMAP data represent difference data. The satellite is positioned at the second Lagrange point of the Sun-Earth system, L2, approximately 1.5 million km from Earth. At this position, the Earth continually shields WMAP from the Sun, as they each complete their orbits. The first year of data collection extended from 10 August 2001 — 9 August 2002, with data release in March 2003. A complete 3-year average data set, spanning 10 August 2001 — 9 August 2004, was released in March 2006.

The WMAP satellite acquires signals at five observational frequencies: 23, 33, 41, 61, and 94 GHz. These are also

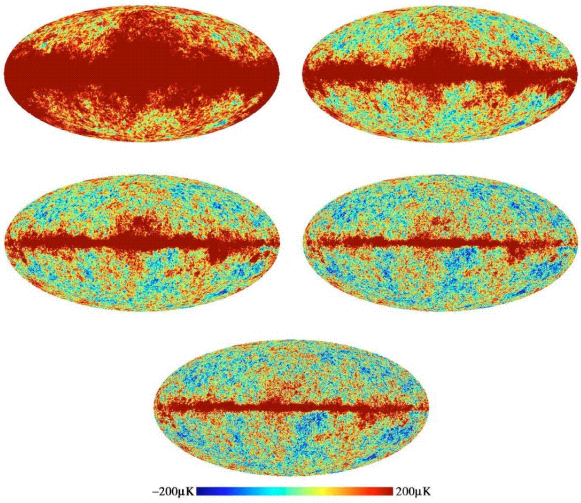


Fig. 1: The five frequency bands observed by the WMAP satellite. Images correspond to 23 GHz (K band, upper left), 33 GHz (Ka band, upper right), 41 GHz (Q band, middle left), 61 GHz (V band, middle right), and 94 GHz (W band, bottom). Reprinted portion of Figure 2 with permission from Tegmark M., de Oliveira-Costa A., Hamilton A.J.S. A high resolution foreground cleaned CMB map from WMAP. *Phys. Rev. D*, 2003, v. 68(12), 123523; http://link.aps.org/abstract/PRD/v68/e123523. Copyright (2003) by the American Physical Society.

known as the K, Ka, Q, V, and W bands. Images generated at these bands are displayed in Figure 1. Final anisotropy maps are prepared by combining the signals represented in Figure 1 with particular weighting at 61 GHz. Maps for each year are prepared individually and then combined "for a number of reasons" [23]. Extensive image processing is applied prior to generating the final anisotropy map (see Figure 2). The noise level in the data sets depends on the number of observations at each point. The major hurdle for WMAP is the presence of the strong foreground signal from our galaxy. In a sense, the WMAP team is trying to "look through" the galaxy, as it peers into the Universe.

In recent years, WMAP results have been widely disseminated both in the scientific literature and the popular press. Nonetheless, there are sufficient questions relative to the manner in which the WMAP data is processed and analyzed, to call for careful scrutiny by members of the imaging community. The implications of WMAP are not only financial and scientific but, indeed, have the potential to impact the course of science and human reason for many generations. As a result, images which are the basis of such specific scientific claims must adhere to standard practices in imaging science. Consequently, and given the precision of the constants provided by WMAP, it is appropriate to review the underlying images and subject them to the standards applied in radiological image analysis. These include most notably signal to noise, resolution, reproducibility, and contrast. These four characteristics represent universally accepted

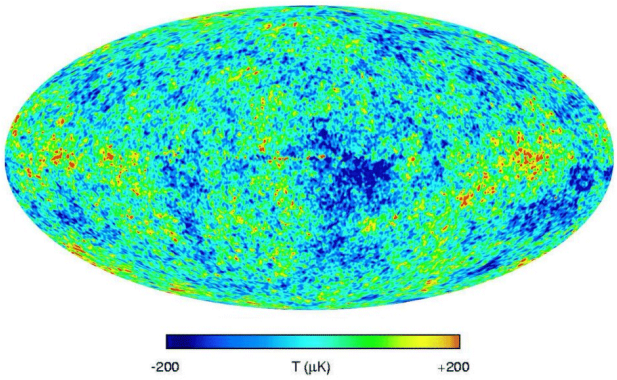


Fig. 2: Cleaned internal linear combination (ILC) map produced by the WMAP team [7]. This image corresponds to Figure 11 in Bennett et. al. [7]. Reproduced with permission of the AAS. Image provided courtesy of the NASA/WMAP team.

measures of image quality. However, before embarking on this exercise, it is important to address dynamic range and the removal of the galactic foreground. In addition, it is useful to review the procedure which the WMAP team employs in image reconstruction.

## 2 Image analysis

### 2.1 Dynamic range and the removal of the Galactic foreground

The WMAP satellite acquires its data in five frequency bands. Five images obtained at these bands (K, Ka, Q, V, and W) are displayed in Figure 1 [29]. The galactic foreground dominates this entire series of images. The foreground is seen as a bright red signal across the central portion of each frequency map. Indeed, the center of the galactic foreground, observed by WMAP, exceeds the desired anisotropic signal in brightness by a factor of $\sim$1,000 [11]. Therefore, the WMAP team is attempting to visualize extremely weak anisotropy in the presence of a much more powerful contaminating signal. This becomes a dynamic range issue analogous to water suppression in biological proton nuclear magnetic resonance (NMR).

Water suppression is an important technique in proton NMR, since most compounds of biochemical interest are typically found dissolved in the aqueous cytosol of the cell. This includes a wide array of proteins, signal messengers, precursors, and metabolic intermediates. Water is roughly 110 molar in protons, whereas the signal of interest to the biochemist might be 1–100 millimolar. In the best case scenario, biological proton NMR, like WMAP, presents a $\sim$1,000 fold problem in signal removal. In the worst case, factors of 100,000 or more must be achieved. Extensive experience in biological NMR obtained throughout the world has revealed that it is impossible to remove a contaminating signal on these orders of magnitude without either (1) ability

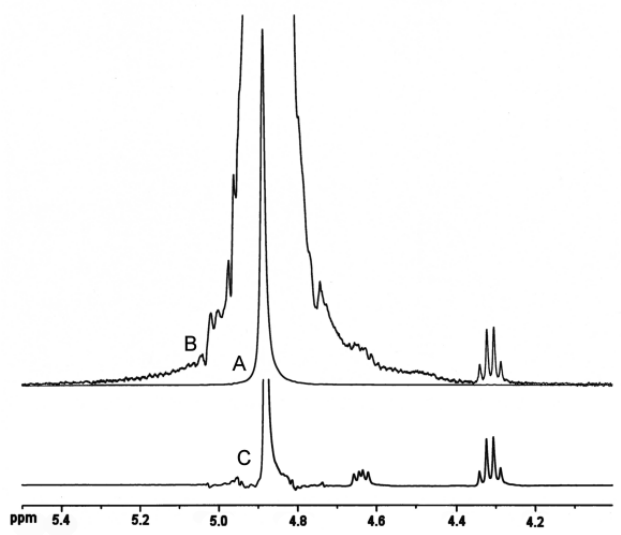


Fig. 3: Proton nuclear magnetic resonance (NMR) spectra acquired from a 0.1 M solution of 0.1 M N-benzoyl-L-arginine ethyl ester hydrochloride in water (A, B). The spectrum is shown in full scale (A). In (B) the vertical axis has been expanded by a factor of 100, such that the resonance lines from the N-benzoyl-L-arginine ethyl ester can be visualized. A $^{1}$H-NMR spectrum acquired from 0.1 M N-benzoyl-L-arginine ethyl ester hydrochloride in deuterium oxide ($D_2O$) is also displayed (C). Spectra display only the central region of interest (4.0–5.5 ppm). Acquisition parameters are as follows: frequency of observation 400.1324008 MHz, sweep width 32,768 Hz, receiver gain 20, and repetition time 5 seconds. The sample dissolved in $D_2O$ (C) was acquired first using a single acquisition and a 90 degree nutation. A field lock was obtained on the solvent. This was used in adjusting the field homogeneity for both samples. For (A) and (B), 20 acquisitions were utilized to enable phase cycling of the transmitter and receiver. In this case, the nutation angle had to be much less than 90 degrees in order not to destroy the preamplifier. A field lock could not be achieved since $D_2O$ was not present in the sample. These slight differences in acquisition parameters and experimental conditions make no difference to the discussion in the text relative to problems of dynamic range.

to affect the signal at the source, and/or (2) *a priori* knowledge. Unfortunately for WMAP, neither of these conditions can be met in astrophysics.

In NMR, ability to effect signal at the source requires direct manipulation of the sample, either biochemically through substitution, or physically, through specialized spin excitation. Biochemical substitution involves the removal of the protons associated with water, using deuterium oxide ($D_2O$) as an alternative solvent [30]. Often, the sample is lyophilized [31]. That is, it is frozen and placed under vacuum so that all of the water can be removed through sublimation. The solvent is then replaced by the addition of $D_2O$. This process can be repeated several times to remove most of the exchangeable protons contained in the sample. The protons are hence replaced by deuterium, which is no longer detectable at the frequency utilized to acquire the desired proton NMR spectrum. Thus, in order to achieve a factor of 1,000 in suppression, the biochemist, in the laboratory, often invokes a rather dramatic modification of the sample at the source.

In Figure 3, a series of $^{1}$H-NMR spectra is presented. Figure 3A corresponds to a mixture of 0.1 M N-benzoyl-L-arginine ethyl ester hydrochloride in water. Since water is 110 M in protons, this solution constitutes roughly a 1,000 fold excess of water protons versus sample protons. Interestingly, the only signal which can be detected in Figure 3A is that of water at 4.88 ppm. The multiple resonances from the N-benzoyl-L-arginine ethyl ester hydrochloride have about the same intensity as found in the line width. In Figure 3B, the same spectrum is reproduced but, this time, the vertical scale has been expanded 100 times. Now, the resonances from the sample are readily observed. The ratio of the water resonance in Figure 3A or B to the quartet at 4.3 ppm is 670. Note, however, that a doublet pair, located at $\sim$4.63 ppm (Figure 3B) is being distorted by the intense resonance line from water. This is easy to assess by examining Figure 3C, wherein a solution of 0.1 M N-benzoyl-L-arginine ethyl ester hydrochloride was reconstituted in 99.8% $D_2O$. In the $D_2O$ spectrum (C), the ratio of the water resonance to the quartet at 4.3 ppm is 21. In this case, the water line is greatly attenuated, since most of the water protons have been replaced with deuterium. Indeed, substitution of $D_2O$ for water (C) results in a 30 fold drop in the intensity of the water line. With this sample, all of the resonances from the N-benzoyl-L-arginine ethyl ester hydrochloride in the vicinity of the water resonance can be visualized, including the doublet pair, at 4.63 ppm. From this information, the ratio of the water to the doublet pair at 4.63 ppm is $\sim$1,500.

Through Figure 3, it is easy to envision the tremendous challenge involved in removing a contaminating signal which dominates the species of interest by $\sim$1,000 fold. In Figure 3B, it is readily apparent that the doublet pair at 4.63 ppm is being distorted by the water line. Consequently, the presence of the intense water resonance affects spins which are adjacent, not only co-resonant. The situation is actually much worse for WMAP as the satellite is attempting to visualize signals contained at the same frequency of observation as the galactic foreground signals. In a sense, the WMAP team is trying to see signals directly beneath the water line, not adjacent to it. To further aggravate the situation, the WMAP team is dealing with extremely weak signals, on the same order of magnitude as the noise floor (see below). Note that the obscured resonances at $\sim$4.63 ppm in the water spectrum would still have a signal to noise of $\sim$5:1, if the water line had not contaminated this region. This can be gathered by comparing Figures 3B and 3C. For WMAP, the signal to noise is less than 2:1, and the signal of interest is located at the same frequency of the contamination.

Relative to dynamic range and removal of a contaminating water signal in NMR however, an alternative to replacing

water with deuterium oxide exists. In fact, it is possible to utilize specialized spin excitation techniques which either exploit the position of the water line in the spectrum [32–36] or invoke gradient and/or multiple quantum selection [37–39]. Indeed, the approaches to water suppression and dynamic range problems in NMR are so numerous that only a few methods need be discussed to adequately provide experimental insight relative to WMAP.

If the experimentalist is not concerned with signals lying at the same frequency of the water resonance, it is sometimes possible to excite the spins in such a manner that the protons co-resonating with water are nulled and other regions of the spectrum are detected [32–36]. This approach is adopted by methods such as presaturation [32], jump-return [33], and other binomial sequences for spin excitation [34–36]. In each case, the spectral region near the water resonance is sacrificed in order to permit the detection of adjacent frequencies. Despite the best efforts, these methods depend on the existence of very narrow water line widths. Water suppression with these methods tends to be limited to factors of $\sim$100. The situation in-vivo might be slightly worse given the wider line widths typically observed in this setting. Despite this apparent success, these methods fail to preserve the signal lying "beneath" the water resonance. Such information is lost.

In certain instances, it is also possible to excite the spectrum by applying specialized gradient-based methods and quantum selection for spin excitation. In so doing, advantage is made of the unique quantum environment of the spins. These methods have the advantage that spins, which co-resonate with water, are not lost. As such, water suppression can be achieved while losing little or no chemical information. The most powerful of these methods often have recourse to gradient fields, in addition to RF fields, during spin excitation [37–39]. These approaches have been particularly important in the study of proteins in solution [39]. Using quantum selection, it is not unreasonable to expect spin excitation with factors of 1,000–10,000 or more in water suppression.

Methods which rely on coherence pathway selection, or hetero-nuclear multiple quantum selection, constitute important advances to NMR spectroscopy in general, and protein NMR in particular [39]. In the absence of these methods, modern aqueous proton NMR would be impossible. In fact, over the course of the last 50 years, it has been amply demonstrated that it is simply not possible to acquire any information of interest, near the water resonance in biological NMR, by data processing a spectrum obtained from an aqueous sample without *a priori* water suppression. Yet, the WMAP map team attempts the analogous data processing feat, in trying to remove the foreground galactic signal.

Unlike the situation in astrophysics, it is possible to address dynamic range issues in NMR, since the spectroscopist literally holds the sample in his hands. The required signals can be selected by directly controlling spin excitation and, therefore, the received signal. Water suppression is addressed prior to signal acquisition, by carefully avoiding the excitation of spins associated with water. The analogous scenario is not possible in astrophysics.

To a smaller extent, water suppression in biological NMR could perhaps be achieved with *a priori* knowledge (i.e. a perfect knowledge of line shapes, intensity, and position). However, such an approach has not yet been successfully implemented in the laboratory. As a result, *a priori* knowledge in NMR is theoretically interesting, but practically unfeasible. This is an even greater limitation in astrophysics where very limited knowledge of the sample exists. The vast experience of NMR scientists demonstrates that the removal of a strong contaminating signal, for the detection of a much weaker underlying signal, is impossible without affecting the signals at the source. Biological NMR has been in existence for over half a century. During most of this time, achieving a factor of 1,000 in signal removal was considered a dramatic achievement, even when combining spin excitation methods with lyophylization. Only in the past 15 years have methods improved, and this solely as a result of gradient-based or multiple-quantum techniques, which provide even more powerful spin selection during excitation [39]. Signal suppression, by a factor of 100, or more, while still viewing the underlying signal, depends on the ability to control the source. This has been verified in numerous laboratories where the sample is known and where the correct answer can be readily ascertained. As such, it is impossible for the WMAP team to remove the galactic foreground given the dynamic range situation between the contaminant and the signal of interest. Attempts to the contrary are futile, as indicated by the need to segment the final images into 12 sections, and alter, from section to section, the linear combination of data, as will be discussed below.

The galactic problem alone is sufficient to bring into question any conclusion relative to anisotropy from both WMAP and COBE. Nonetheless, additional insight can be gained by examining image reconstruction.

### 2.2 ILC image reconstruction

#### 2.2.1 Combining section images

Despite this discussion relative to NMR, the WMAP team claims that removal of the galactic foreground is possible and therefore proceeds to ILC image generation. As mentioned above, the WMAP satellite obtains its data in five frequency bands (23, 33, 41, 61, and 94 GHz). In order to achieve galactic foreground removal, the WMAP team utilizes a linear combination of data in these bands, essentially adding and subtracting data until a null point is reached. In doing so, the WMAP team is invoking *a priori* knowledge which cannot be confirmed experimentally. Thus, the WMAP team makes the assumption that foreground contamination

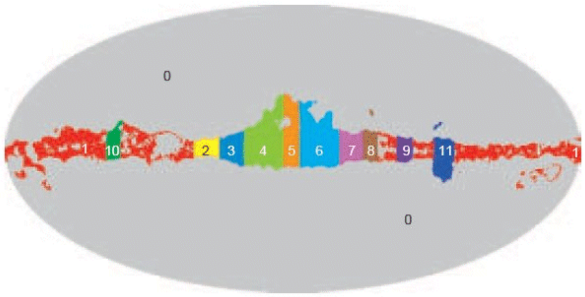


Fig. 4: Illustration of the 12 regions used to generate the ILC maps for year 3 average data. This image corresponds to the upper portion of Figure 8 in Hinshaw et. al. [23]. Reproduced with permission of the AAS. Image provided courtesy of the NASA/WMAP team.

is frequency dependent, while the anisotropy is independent of frequency. This approach, however, is completely unsupported by the experimental data, as will be discussed further below.

Furthermore, galactic foreground removal cannot be achieved with a single linear combination of data. Rather, WMAP achieves its final maps by first generating separately processed section images. Eleven of these regions lie directly in the galactic plane, as shown in Figure 4. Each section is processed individually. The twelve processed section images are then combined and smoothed to generate the final ILC maps.

The WMAP team invokes completely different linear combinations of data to process adjacent regions of the galactic plane. In medical imaging, there is seldom, if ever, the need to process final images in sections. Given this fact, note the processing applied to generate regions 4 and 5 in the 3-year average data (see Figure 4). The coefficients, for section 4, correspond to $-0.0781$, $0.0816$, $-0.3991$, $0.9667$, and $0.4289$ for the K, Ka, Q, V, and W bands, respectively [23]. In sharp contrast, the coefficients for section 5 correspond to $0.1839$, $-0.7466$, $-0.3923$, $2.4184$, and $-0.4635$, for these same bands [23]. The WMAP team alters the ILC weights by regions, used in galactic signal removal, by more than a factor of 100% for the fourth coefficient, despite the adjacent locations of these sections. The same problem exists for several other adjacent sections in the galactic plane [23]. The sole driving force for altering the weight of these coefficients lies in the need to zero the foreground. The selection of individual coefficients is without scientific basis, with the only apparent goal being the attainment of a null point. The full list of ILC coefficients adopted by the WMAP team are reproduced in Table I (reprint of Table 5 in reference [23]). Analysis of this table reveals the tremendous coefficient variability used, from section to section, for zeroing the galactic foreground.

In generating the ILC maps, the WMAP team chose to primarily weigh the V-band. As a result, the coefficients selected tend to reflect this emphasis. However, there is no

| Region | K-band | Ka-band | Q-band | V-band | W-band |
|---|---|---|---|---|---|
| 0 | 0.1559 | −0.8880 | 0.0297 | 2.0446 | −0.3423 |
| 1 | −0.0862 | −0.4737 | 0.7809 | 0.7631 | 0.0159 |
| 2 | 0.0358 | −0.4543 | −0.1173 | 1.7245 | −0.1887 |
| 3 | −0.0807 | 0.0230 | −0.3483 | 1.3943 | 0.0118 |
| 4 | −0.0781 | 0.0816 | −0.3991 | 0.9667 | 0.4289 |
| 5 | 0.1839 | −0.7466 | −0.3923 | 2.4184 | −0.4635 |
| 6 | −0.0910 | 0.1644 | −0.4983 | 0.9821 | 0.4428 |
| 7 | 0.0718 | −0.4792 | −0.2503 | 1.9406 | −0.2829 |
| 8 | 0.1829 | −0.5618 | −0.8002 | 2.8464 | −0.6674 |
| 9 | −0.0250 | −0.3195 | −0.0728 | 1.4570 | −0.0397 |
| 10 | 0.1740 | −0.9532 | 0.0073 | 2.7037 | −0.9318 |
| 11 | 0.2412 | −1.0328 | −0.2142 | 2.5579 | −0.5521 |

Table 1: ILC weights by regions. ILC coefficients used in the analysis of 3-year data by the WMAP team. This table corresponds to Table 5 in Hinshaw et. al. [23]. Utilized courtesy of the NASA/WMAP team.

*a priori* reason why the weighting could not have emphasized the Q band, for instance. This is especially true since anisotropy is advanced as being frequency independent. Indeed, it is interesting that the Q and W bands have coefficients on the order of $-0.4$, while lying in proximity to the V band which is given a weight of 2.4 for region 5.

Nonetheless, the scientifically interesting region in the ILC map corresponds to section 0 (see Figure 4). Thus, problems in removing the galactic foreground could be tolerated, given that the WMAP team has no other alternative. It is the processing utilized for section 0 which is most important. This brings yet another complication. Completely different ILC maps of the Universe would be obtained, if the WMAP team had decided to emphasize a frequency other than the V band. In that case, an altered set of cosmological constants is very likely to be generated, simply as a result of data processing.

In removing the galactic foreground, the WMAP team has assumed that the anisotropy is frequency independent. In reality, it is already clear that an ILC map generated with weighting on the Q-band, for instance, will be dramatically different. The requirement that the signals of interest are frequency independent cannot be met, and has certainly never been proven.

In the first data release, the only real requirement for generating the ILC maps was that the coefficients sum to 1. As such, an infinite number of maps can be generated. There is no single map of the anisotropy, since all maps are equally valid, provided coefficients sum to 1. In this regard, alternative anisotropic maps have been presented [29]. Tegmark et. al. [29] generate a new anisotropy map by permitting

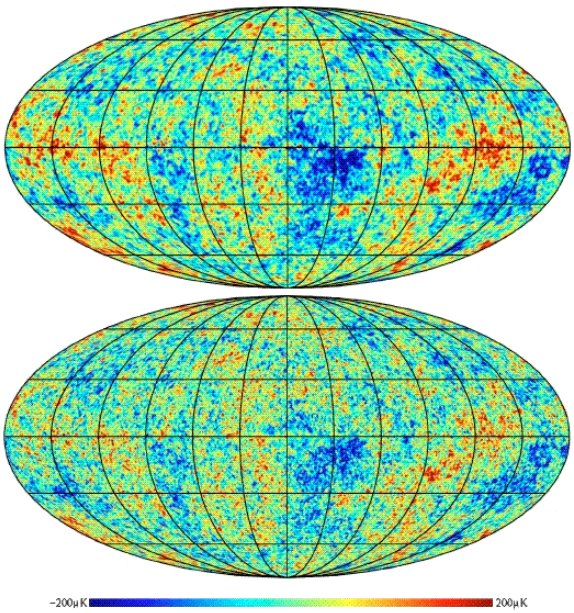


Fig. 5: Cleaned internal linear combination (ILC) anisotropy map produced by the WMAP team (top) and Wiener filtered anisotropy map (bottom) produced by Tegmark et. al. [29]. Reprinted portion of Figure 1 with permission from Tegmark M., de Oliveira-Costa A., Hamilton A.J.S. A high resolution foreground cleaned CMB Map from WMAP. *Phys. Rev. D*, 2003, v. 68(12), 123523; http://link.aps.org/abstract/PRD/v68/e123523. Copyright (2003) by the American Physical Society.

the coefficient weighting to depend both on angular scale and on distance to the galactic plane. This approach was substantially different from that implemented by the WMAP team and it reinforces the finding that no single anisotropy map exists. In Figure 5, it is apparent that the map generated by the WMAP team (top) does not agree with the map generated by Tegmark et. al. (bottom) [29].

An infinite number of maps can be generated from the 5 basis sets. There is no unique solution and therefore each map is indistinguishable from noise. There are no findings relative to anisotropy, since there are no features in the maps which could guide astrophysics relative to the true solution.

With the release of the 3-year data set however, the WMAP team claims that they can use mathematical methods to find the maximum likelihood sky map [23]. Unfortunately, there are no means to test the validity of the solution. In this regard, astrophysics is at a significant disadvantage relative to clinical MRI. Thus, the radiological scientist is guided by known anatomy, and by the results of all other imaging modalities focused on the same sample. This is not the case in astrophysics, since no single spectroscopic frequency holds an advantage over any other. There is no "known" signature to guide the choice of coefficients. A map might appear to be favored, however, devoid of secondary experimental verification, its legitimacy can never be established. Alternative methods could produce alternative maximum likelihood maps. Another level of testing is being added. Nonetheless, the conclusion remains that an infinite number of maps can be generated since, given sufficient resources, one can generate a number of maximal likelihood approaches with no clear way of excising the "true" solution. Therefore, any discussion relative to the cosmological significance of these results is premature.

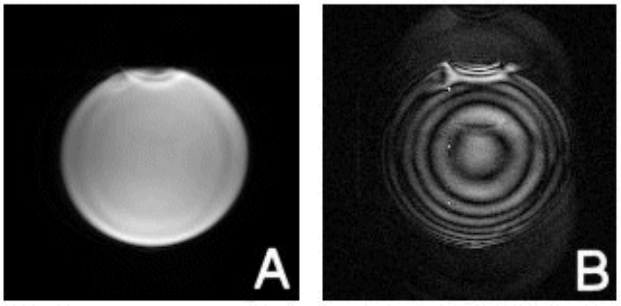


Fig. 6: Ultra High Field 8 Tesla MRI image of an 18 cm ball of mineral oil acquired using a 3-dimentional acquisition. A) Axial slice representing a region contained within the physical space occupied by the 18 cm mineral oil ball. (B) Axial slice through a region located outside the physical space occupied by the ball. Note that the image displayed in (B) should be entirely devoid of signal. The severe image processing artifacts contained in (B) are a manifestation that the processing of powerful signals can result in the generation of weak spurious ghost signals.

### 2.2.2 Generation of spurious signals

Attempts to remove, by signal processing, a powerful galactic signal will invariably generate unwanted features in the maps, indistinguishable from real findings. The process of removing an intense signal can result in the unexpected creation of many spurious weak ghost signals, at any point in the image plane. Therefore, it is crucial that the signal to noise, in the final image or spectrum of interest, be significant.

In biological NMR, the post-water suppression spectrum typically has good signal to noise. It would not be unusual to achieve 1,000 fold suppression of the water signal and obtain a spectrum with a signal to noise well in excess of 10, or even 100, for the species of interest. This signal to noise is high enough to differentiate it from spurious ghost signals, generated either directly by suppression or through data processing.

In MRI, it is well established that the processing of large signals can lead to spurious signal ghosts throughout an image or a set of images. This is displayed in Figure 6. Figure 6A shows an MRI image of an 18 cm phantom sample containing mineral oil. This image is part of a much larger group of images obtained during a 3D test study. In Figure 6B, a series of signal rings are observed. These rings are spurious ghosts. They were produced by obtaining a 3-dimensional data set on an 18 cm ball containing mineral oil, using an 8 Tesla MRI scanner [40–42]. The signal is acquired

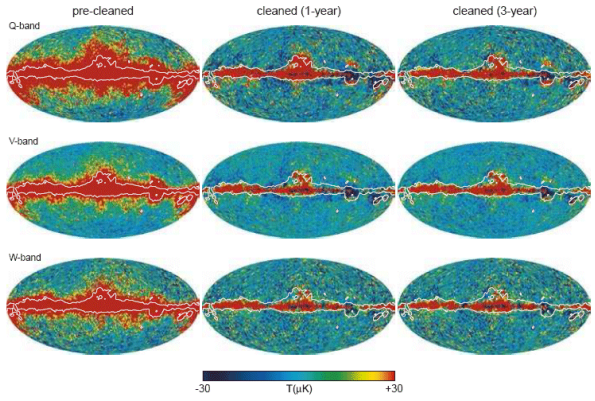


Fig. 7: Illustration of galactic foreground removal for year-1 and for the 3-year average. "Cleaning" is illustrated for the Q, V, and W bands. Similar data are not presented for the K and Ka bands [23]. This image corresponds to Figure 10 in Hinshaw et. al. [7]. Reproduced with permission of the AAS. Image provided courtesy of the NASA/WMAP team.

from the entire ball in the time domain and then Fourier transformed to achieve a set of images in the frequency domain [43]. *The image displayed in Figure 6B corresponds to an imaging slice which lies outside the actual physical space occupied by the ball.* Ideally, this image should be completely black. The spurious signal is a manifestation of a truncation artifact in Fourier transformation during data processing. There should be no signal in this image. However, for the sake of this discussion, it provides an excellent illustration of what can happen when powerful signals must be mathematically manipulated to generate final images.

While the WMAP team is not using simple Fourier transformation to process their images, this lesson nonetheless applies. When mathematically manipulating large signals, weak spurious signals can be created. This phenomenon is common to all image processing, and hence the importance of relatively strong signals of interest once the contaminating signal is removed. This is not the case for WMAP. The contaminating foreground is $\sim$1,000 times the "signal" of interest. Yet, the final signal to noise is poor.

The WMAP team invokes the "cleaning" of its raw images acquired at the K, Ka, Q, V, and W bands prior to presenting the images for these bands [7]. The affect of "cleaning" is demonstrated in Figure 7. Note how the process of "cleaning" the images appears to remove the galactic foreground for the Q, V, and W bands. Interestingly, similar images are not being presented for cleaning the K and Ka bands. This is precisely because the galactic signal contamination is so significant for these two bands. Indeed, the WMAP team needs to present the data for the K and Ka bands in this same figure, in order to place the galactic signal contamination and the associated "cleaning" in proper perspective.

While the galactic center appears to affect only a central region of the Q, V, and W bands in the cleaned image, the situation is more complex. In fact, it is impossible to discern if a given signal is truly independent of the galaxy at any location on the image. This is because the process of "cleaning" images, to remove powerful contaminating signals, is never clean. Mathematical manipulation of powerful signals, whose attributes are not fully characterized or understood, will invariably lead to the generation of image ghosts. Through "cleaning", the WMAP team is taking the risk that it is generating image ghosts. The removal of powerful signals, at certain image locations, can easily be associated with the generation of weak signals at the same (or other) image locations, just as a result of processing. The lesson from Figure 6 applies.

Consequently, the WMAP team is unable to distinguish whether the "features" found in its images are truly of cosmological importance, or whether these features are simply the result of processing (and/or acquiring) a much larger contaminating signal from the galaxy. It is clear, for instance, that K band reveals galactic signal at virtually every point in the sky map (see Figure 1). The same contaminations must be expected in all other bands. That the human eye fails to visualize contamination does not mean that contamination is absent. Because any real signal will be weak, and the contaminating signal is so strong, the WMAP team is unable to distinguish spurious ghosts related to either processing or acquisition from the actual signal of interest. This is true at every image location.

Data processing artifacts tend to be extremely consistent on images. Since similar mathematical methods must be utilized to clean the raw images and zero the galactic foreground, it is highly likely that a significant portion of the maps contains such spurious ghosts. This is especially true given that the WMAP team has chosen to invoke complex mathematical methods for "cleaning" their raw images. That a given image location cannot be positively ascertained to be free of contamination implies that none of the image locations can be validated as free of galactic ghosts on any map. Therein lies the overwhelming complication of dealing with powerful contaminating signals while trying to examine weak ones. Apparent anisotropy must not be generated by processing.

### 2.2.3 Signal to noise, contrast, and resolution

There is perhaps no more important determinant of image quality than signal to noise. In medicine, signal to noise can directly impact diagnosis. As such, radiological methods which are rich in signal to noise are always sought. If signal to noise is high ($>$100:1), then image quality will almost certainly be outstanding. Methods which have high signal to noise can "burn signal" to generate either contrast, resolution, or shortened exam times. Consequently, signal to noise is paramount. Without it, resolution will remain poor and

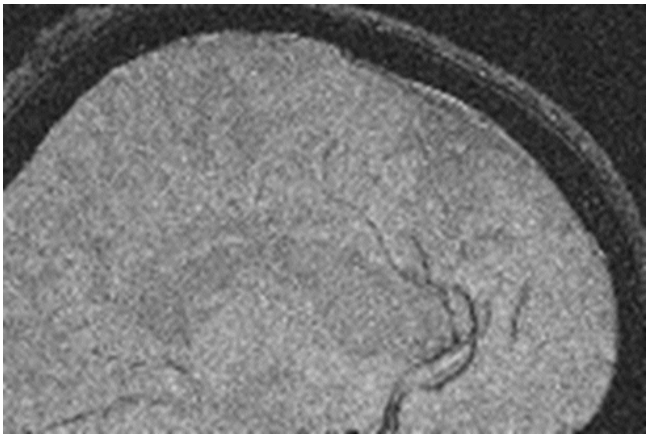

Fig. 8: Section (490 × 327) of a high resolution sagittal image of the human head acquired at 1.5 Tesla. Acquisition parameters are as follows: acquisition sequence = gradient recalled echo, matrix size = 512 × 512, slice thickness = 2 mm, field of view 20 cm × 20 cm, repetition time = 750 msec, echo time = 17 msec, and nutation angle = 45 degrees.

contrast will rapidly deteriorate. In fact, enhancements in signal to noise were the primary driving force for the introduction of Ultra High Field MRI [40–42].

In order to gain some insight into the importance of signal to noise, one can examine the images displayed in Figures 8 and 9. Figure 8 corresponds to a sagittal section of a human brain, acquired using a 1.5 Tesla MRI scanner. There are more than 15,000 such scanners in existence. In this image, the 1.5 Tesla instrument was brought to the very limits of its performance [43]. The resolution is high (matrix size = 512 × 512) and the slice thickness is thin (2 mm). At the same time, the nutation angle, echo times, and repetition times are all suboptimal. As a result, this image is of extremely poor clinical quality. The contrast between grey and white matter has disappeared and the signal to noise is $\sim 5$.

Figure 9 was acquired with the first UHFMRI scanner [40–42]. This scanner operates at a field strength of 8 Tesla. Note the phenomenal contrast, the delineation of grey and white matter and the appearance of vasculature. Interestingly, this image was acquired with a much larger image resolution (matrix size = 2,000 × 2,000) while maintaining nearly the

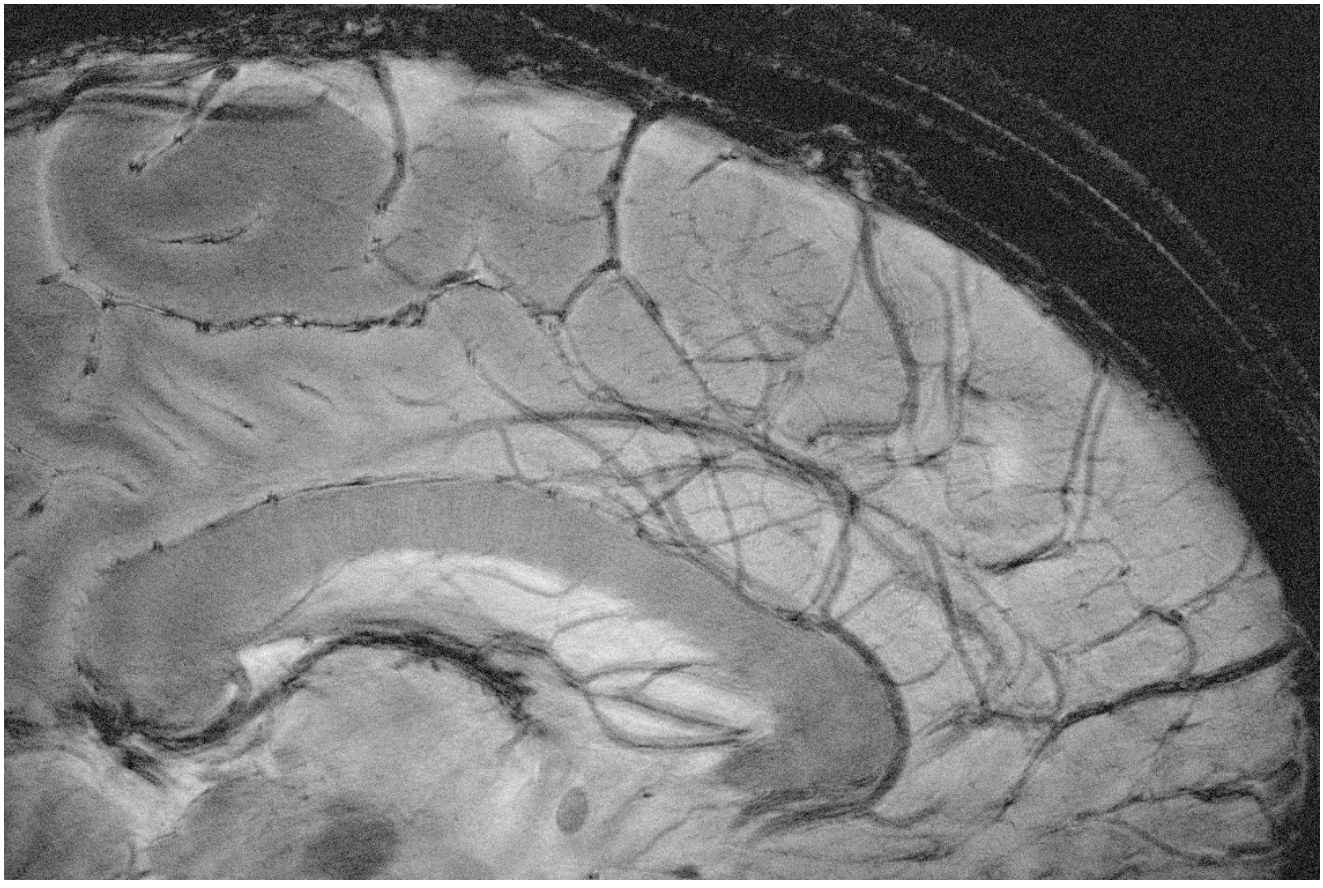

Fig. 9: Section (1139 × 758) of a high resolution sagittal image of the human head acquired at 8 Tesla. Acquisition parameters are as follows: acquisition sequence = gradient recalled echo, matrix size = 2,000 × 2,000, slice thickness = 2 mm, field of view 20 cm × 20 cm, repetition time = 750 msec, echo time = 17 msec, and nutation angle = 17 degrees. This image corresponds to Figure 3A in Robitaille P.M.L., Abduljalil A.M., Kangarlu A. Ultra high resolution imaging of the human head at 8 Tesla: 2K×2K for Y2K. *J Comp. Assist. Tomogr.*, 2000, v. 24, 2–7. Reprinted with permission.

same parameters as found for Figure 8. Despite higher resolution, the image has a signal to noise of ∼20. It did take longer to acquire, due to increased phase encoding steps, but the time per pixel remains less than that for Figure 8. Clearly, signal to noise can purchase both contrast and resolution.

Images with high signal to noise also tend to be "reliable". Namely, their gross features are rarely affected by minor fluctuations, in either the instrument or the sample. High signal to noise images tend to have the quality of stability and reproducibility, attributes which are often lost in low signal to noise images. In fact, the only measure of reliability for a low signal to noise image is reproducibility. It is important to establish that a low signal to noise image does not change from one acquisition to the next.

Figure 10A-C displays three low signal to noise images. In these images, a computer has added random noise, such that the final signal to noise is ∼2.5:1 in each case. Figure 10A corresponds to an axial image of the human head. Its identity is revealed by the presence of signal arising both from the brain and the scalp. The image is relatively uniform in signal, making the assignment simple. Figure 10B corresponds to a photograph of the Moon. The subject can be distinguished from other spherical objects (a baseball, the Sun, etc.) through the gentle change in contrast, produced by craters on the lunar surface. The object is difficult to identify since the shape provides few clues. Figure 10C corresponds to an MRI image of the author's wrist. In this image, it is increasingly difficult to ascertain the source. The maximal signal to noise remains ∼2.5:1. However, the signal distribution is no longer uniform. Faint features can be seen on the image, but no detail. Inhomogeneous signal distributions often make images more challenging to interpret, particularly when the origin of the sample is not known.

In Figure 11A-C, the images of Figure 10A-C are reproduced, but this time the signal to noise is at least 5:1. A nearly 10-fold increase in signal to noise for the head image (A) is now associated with increased contrast. The same holds true for the wrist image displayed (C) with a signal to noise of ∼40:1. Thus, the first rule of image contrast is that it is non-existent on low signal to noise images. It takes signal to make contrast. If the images in Figure 11 look so much more appealing, it is because they have higher signal to noise and contrast. It is also interesting that a mere doubling of signal to noise has such a dramatic effect for the Moon image. This highlights that there is also an enormous difference between an image with a 1.5:1 signal to noise and an image with a 2.5:1 signal to noise.

Unfortunately, in the WMAP images, the maximum signal to noise is just in excess of 1. This can be ascertained in Figures 12 and 13. Figure 12 displays a map of instrument noise released by NASA for WMAP. The largest signals on this map have a noise power of approximately 70 uK. Figure 12 displays a corresponding map, created by combining the Q and V bands. The galactic plane dominates the figure with

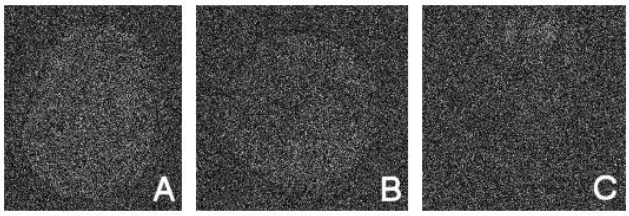


Fig. 10: A set of images generated by adding random noise to the images displayed in Figure 11. A maximum signal to noise of ∼2.5:1 is now illustrated. (A) MRI image of the human head at 1.5 Tesla, (B) photographic image of the Moon, and (C) MRI image of the author's wrist acquired at 8 Tesla.

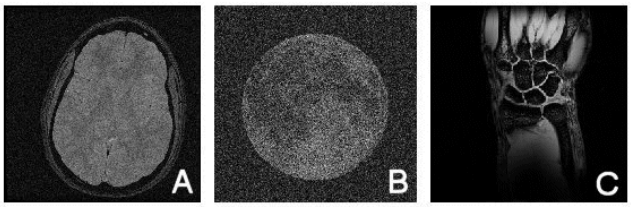


Fig. 11: Images displaying varying signal to noise. (A) MRI image of the human head at 1.5 Tesla with signal to noise ∼20:1, (B) photographic image of the Moon with the signal to noise adjusted to ∼5:1, and (C) MRI image of the human wrist acquired at 8 Tesla with the signal to noise ∼40:1. Note the dramatic effect on image quality for the moon image (B) in simply doubling the signal to noise (see Figure 10B).

signal truncated at the 100 uK level. Outside the galactic plane, few signals, if any, exist at the 100 uK level. As such, by combining the information in Figure 13 with the image in Figure 12, it is clear that the WMAP signal to noise is below 2:1 and probably below 1.5. In fact, since these images are obtained by difference methods, the signal to noise at many locations is much less than 1. It is clear that some of the data points on these images have signal values of 0. Therefore, the real signal to noise on the anisotropy maps is somewhere between 0 and 1.5 at all locations. Note, in contrast, that the example images in Figures 10A, B, and C had a maximum signal to noise of ∼2.5:1, well in excess of WMAP and without the presence of a contaminating foreground.

Relative to signal to noise, the WMAP team is unable to confirm that the anisotropic "signal" observed at any given point is not noise. The act of attributing signal characteristics to noise does not in itself create signal. Reproducibility remains the key, especially when signal to noise values are low.

### 2.2.4 Reproducibility

The presence of low signal to noise on an image is not unusual in science, and many a great discovery has been made through the careful analysis of the faintest signals. In medicine, the tremendous advancements in functional MRI mapping of the brain [44–46] stand perhaps without rival,

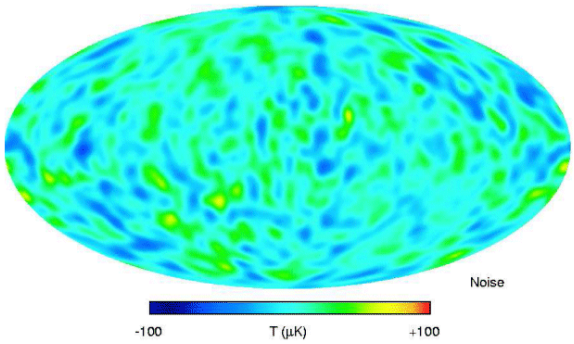


Fig. 12: Map of the instrument noise for WMAP. This image corresponds to the lower portion of Figure 9 in Bennett et. al. [7]. Reproduced with permission of the AAS. Image provided courtesy of the NASA/WMAP team.

relative to lack of signal to noise and the profoundness of the implications. Whenever the signal to noise is low, care must be exercised such that noise is not mistaken for signal. The key to this problem is reproducibility.

In medicine, when an image has poor signal to noise, it is vital that its central features be reproducible.

In fact, the only measure of reliability for a low signal to noise image is reproducibility. The information contained within the image must not change from one acquisition to the next. Correlation between an event and the change in an image are also powerful indicators that the change is real. This principle has been applied extensively in human functional MRI [44–46]. In this case, cognitive tasks, such as visual activation or finger tapping, can be directly correlated to very small changes on the MRI images of the human brain [44–46]. Often, changes on a pixel by pixel basis, with a signal to noise change on the order of 5:1 or even less, can be trusted simply based on correlation. In medicine, whenever a known physiological change (blood flow, blood oxygenation level, and myocardial contraction) can be correlated to radiological changes, even low signal to noise images can yield powerful diagnostic conclusions. Three components in this case act in unison to produce the diagnosis: instrument stability, image reproducibility, and the presence of correlation.

Note, most importantly, that in medicine, when low signal to noise images are used for diagnosis, it is never in the presence of strong overlapping contaminating signal. Moreover, in human functional imaging, a set of control images are acquired to help ensure that all perceived changes are real.

Unfortunately for WMAP, not only are the images obscured by galactic contamination, but they do not appear to be reproducible. In this regard, it is concerning that the WMAP team chooses to alter the ILC coefficients for generating section 0 from year to year. In fact, the coefficients used in year-1 (0.109, −0.684, −0.096, 1.921, and −0.250) are substantially different from those used in presenting a 3-year average (0.1559, −0.8880, 0.0297, 2.0446, and

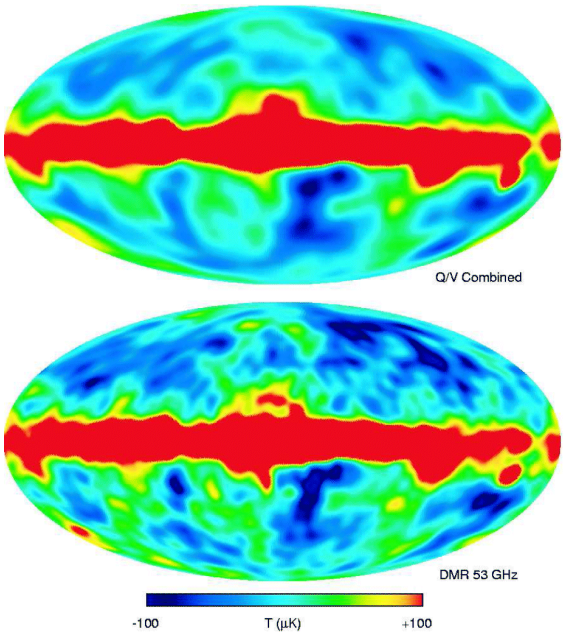


Fig. 13: The 53 GHz map from COBE (bottom) and the combined Q/V map generated by the WMAP team. This Figure corresponds to Figure 8 in Bennett et. al. [7]. Reproduced with permission of the AAS. Image provided courtesy of the NASA/WMAP team.

−0.3423). The coefficient for K band has changed by nearly 50%, while the coefficient for Q band not only changes sign, but decreases in magnitude by a factor of 3. Such changes cannot be simply explained by variations in instrument gain over time. The WMAP team does describe an attempt to find the maximum likelihood map in the 3-year data presentation. This new approach may account for some of the variability. Nonetheless, the WMAP team should have reprocessed the data from all years using this new approach, so that a direct comparison could be made between images processed with identical parameters.

It is also concerning that the WMAP team does not present separate ILC images for years 1, 2, and 3. Rather, after presenting the year-1 ILC image in 2003, they then compare it only to the 3-year average in 2006. However, the 3-year average contains data from the first year. The proper test for reproducibility involves the comparison of each yearly ILC image with one another, without invoking the 3-year average. Ideally, difference ILC images should be taken from year-1 and year-2, year-2 and year-3, and finally from year-1 and year-3. The WMAP team neglects to present these vital comparisons.

Despite these objections, the first year image simply does not agree with the 3-year average. It is true that the images generally agree, but this does not occur on a pixel by pixel, or even a regional basis. This can be readily visualized in the difference images displayed in Figures 14 and 15. In fact, the situation is actually worse than can be easily gathered, since the coefficients used in generating the first year ILC maps

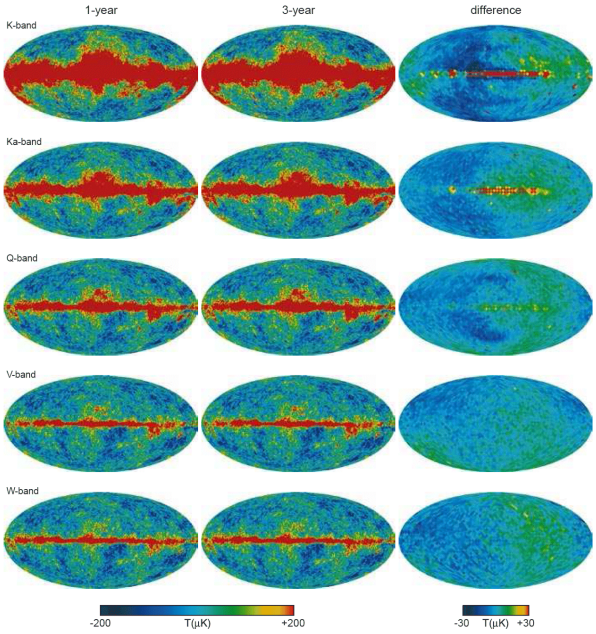


Fig. 14: Comparison of 3-year average data with year-1 data through difference for the K, Ka, Q, V, and W bands of the WMAP satellite. Note that the difference images are shown with reduced resolution contrary to established practices in imaging science. This figure corresponds to Figure 3 in Hinshaw et. al. [23]. Reproduced with permission of the AAS. Image provided courtesy of the NASA/WMAP team.

do not agree with those used for the 3-year average map. The comparison made by the WMAP team in Figure 15 is not valid, since the images were generated using different coefficients.

Perhaps most troubling, the WMAP team chooses to reduce the resolution on its difference images. This approach is known to minimize apparent differences. In imaging, the only resolution which can be claimed is that which can be trusted on difference. As such, if the difference images must be degraded to a pixel resolution of 4 degrees, then the WMAP team cannot claim to have imaged the sky at a 1 degree resolution.

Tremendous variability can be observed in the WMAP data sets. This is apparent by examining the variability found in the galactic foreground. It has been well established in astrophysics that galaxies can contain Active Galactic Nuclei. These have been studied extensively outside the microwave region [47]. These nuclei can vary by an order of magnitude in certain frequency bands [47]. Even in the microwave, it is clear that our own galaxy is highly variable from year to year. This is evidenced by the need to change, from year to year, the coefficients required to null the galactic contribution. The galaxy is highly variable in the microwave relative to the magnitude of any real anisotropy. This is an observation which could be made by examining old data from COBE [48]. Given this state, it is also clear that every galaxy in the

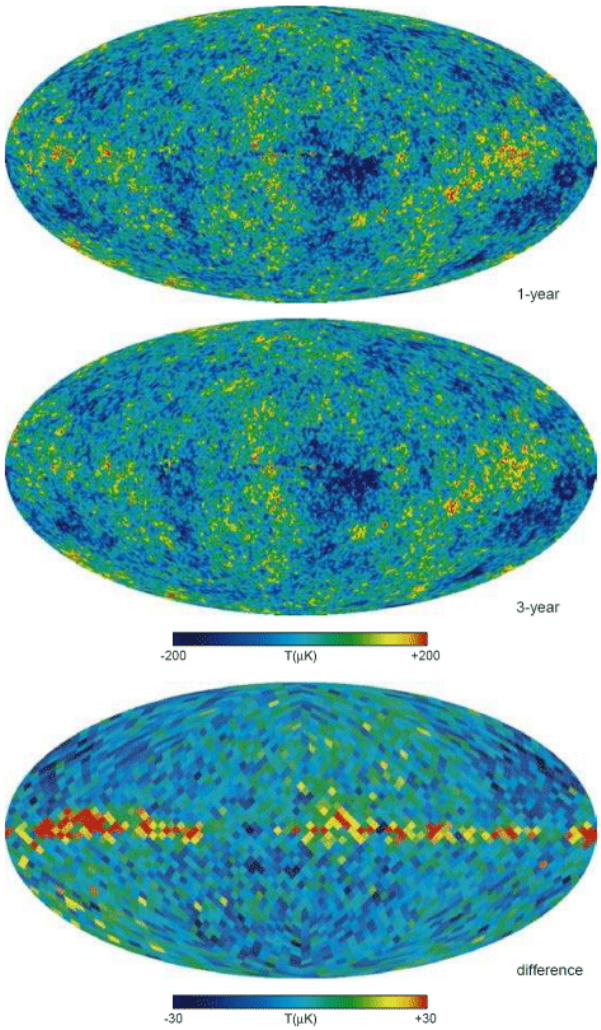


Fig. 15: Comparison of the 3-year average ILC map with the year-1 ILC map. Note that the difference images are shown at reduced resolution contrary to established practices in imaging science. This figure corresponds to Figure 9 in Hinshaw et. al. [23]. Reproduced with permission of the AAS. Image provided courtesy of the NASA/WMAP team.

Universe will also share in this variability in a manner which is completely dissociated from any cosmological implication. Indeed, herein lies another great problem for the cosmologist. It is impossible to visualize, in our lifetime, the true simple galactic variability not only from our galaxy, but from every other galaxy. Even a signal which appears stable over the course of humanity's existence may well be variable.

Consider the case where only 4 pixels vary substantially over the course of the WMAP experiment from year-1 to year-4. From this situation, it can be expected that as many as 1,000 pixels might vary over the course of 1,000 years. Yet, 1,000 years is barely on the cosmological timescale. Over the course of 1,000,000 years, a total of 1,000,000 pixels could be potentially affected. Even 1,000,000 years is just starting to be meaningful relative to cosmology. As a

result, the situation relative to WMAP and COBE is extremely difficult. In reality, in order to have true cosmological meaning, the maps must be temporally stable well beyond what has been determined to date. The situation is much worse than the hypothetical case described above, as significantly more than 4 pixels will vary between year-4 and year-1. The requirements for image stability in cosmology is well beyond the reach of both COBE and WMAP.

### 2.3 The flat model of the Universe

Bennett et. al. [7] claim that the WMAP results are consistent with a 2-dimensional flat model of the Universe. Clearly, by their intrinsic nature, these images are incapable of supporting any higher order model. WMAP cannot establish the origin of the photons which it detects other than in a directional sense. The satellite is completely unable to differentiate data based on distance to the source. In this respect, WMAP images resemble classic X-rays in medicine. Such images are 2-dimensional and unable to reveal the 3-dimensional nature of the human being. WMAP and X-rays stand in sharp contrast to the CT and MRI systems of today, which are able to provide a true 3-dimensional visualization of the human body. That the flat model of the Universe can be fitted is completely appropriate, given that this data cannot be utilized to model a 3-dimensional Universe.

### 2.4 The assignment of brightness temperature

Perhaps the most serious concern relative to the Penzias and Wilson, COBE, and WMAP findings involves the assignment of brightness temperatures [49]. The Universe is not in thermal equilibrium with a perfectly absorbing enclosure [49, 50, 51, 52]. As a result, the assignment of these temperatures constitutes a violation of Kirchhoff's Law [50, 52]. It is improper to assign a temperature merely because a spectrum has a thermal appearance. That a spectrum appears thermal does not imply that it was generated by a blackbody [52, 53]. Indeed, the proper application of the laws of Planck [54], Stefan [55], and Wien [56] requires that the emitting sample corresponds to a solid, best approximated on Earth by graphite or soot [50]. It has been advanced [49, 57–59], and it is herein restated, that the monopole signal first detected by Penzias and Wilson, and later confirmed by COBE, will eventually be reassigned to the oceans of the Earth. The brightness temperature does not appear to make any sense precisely because the oceans fail to meet the requirements set forth by Kirchhoff in assigning a temperature [50, 52, 53].

In this regard, the basis of universality in blackbody radiation has come under serious question [52, 53]. Blackbody radiation is not universal. Rather, it is strictly limited to an experimental setting which, on Earth, is best approximated by graphite and soot [52]. That Kirchhoff interchangeably used either an adiabatic enclosure or an isothermal one was a natural extension of his belief in universality. Nonetheless, it appears that the adiabatic case is not valid [52]. Kirchhoff's experiments far from supporting universality, actually constrains blackbody radiation to the perfect absorber [52]. Conditions for assigning a blackbody temperature are even more stringent [52] than previously believed [58]. As such, an adiabatic enclosure is not sufficient [52, 58]. Rather, in order to obtain a proper temperature, the enclosure can only be perfectly absorbing and isothermal. The assignment of these temperatures by the WMAP team constitutes an overextension of the fundamental laws which govern thermal emission, given the lack of universality [52, 53].

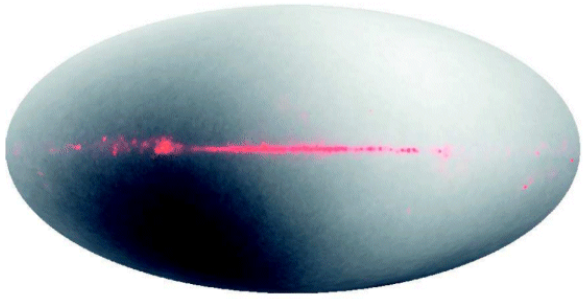

Fig. 16: The microwave dipole observed by the WMAP satellite. This image corresponds to the upper portion of Figure 10 in Bennett et. al. [7]. Reproduced with permission of the AAS. Image provided courtesy of the NASA/WMAP team.

### 2.5 The Dipole Temperature

Despite this discussion, it is nonetheless clear that the WMAP satellite has detected a CMB dipole signal presumably associated with motion of the local group [7, 23]. The dipole signal is shown in Figure 16. The presence of a dipole is thought, by many, as further proof for the presence of the monopole signal at the position of WMAP. The detection of this dipole by WMAP constitutes a finding of importance as it confirms earlier findings, both by the COBE team [60] and by the Soviet Relikt-1 mission [61]. Indeed, the discussion of the dipole is sufficiently important to be treated separately [62].

## 3 Conclusion

Analysis of data from WMAP exposes several problems which would not be proper in medical imaging. Experience from NMR spectroscopy relative to biological samples reveals that removal of a contaminating signal, which exceeds the signal of interest by up to a factor of 1,000, requires ability to control the sample at the source. This requirement can never be met by the WMAP team. It is impossible to remove this contamination and thereby "see beyond the galaxy". It is also dangerous to mathematically manipulate large signals during image reconstruction, especially when the final images have low signal to noise ratios. The

galactic signal is not stable from year to year, making signal removal a daunting task as seen by the yearly changes in ILC coefficients for regions 1–11. In actuality, the WMAP team must overcome virtually every hurdle known to imaging: foreground contamination and powerful dynamic range issues, low signal to noise, poor contrast, limited sample knowledge, lack of reproducibility, and associated resolution issues. It is clear that the generation of a given anisotropy map depends strictly on the arbitrary weighting of component images. The WMAP team attempts to establish a "most likely" anisotropy map using mathematical tools, but they have no means of verifying the validity of the solution. Another team could easily produce its own map and, though it may be entirely different, it would be equally valid. Figure 5 points to this fact. It remains surprising that separate ILC maps are not presented for years 1, 2, and 3. In addition, the WMAP team does not use the proper tests for reproducibility. Difference images between all three yearly ILC maps should be presented, without lowering the final resolution, and without changing the ILC coefficient from year to year. It is improper to compare images for reproducibility if they are not processed using identical methods. Reproducibility remains a critical issue for the WMAP team. This issue will not be easily overcome given human technology. In order to make cosmological interpretations, the WMAP images must be perfectly stable from year to year. Even fluctuation at the level of a few pixels has dramatic consequences, since the data must be stable on a cosmological timescale. This timescale extends over hundreds, perhaps thousands, or even millions of years. Finally, there are fundamental issues at stake, relative to the application of the laws of Kirchhoff [50], Planck [54], Stefan [55], and Wien [56]. It has not been established that the WMAP team is theoretically justified in assigning these temperatures.

The only significant observations relative to this satellite are related to the existence of a dipole signal [7, 23]. This confirms findings of both the NASA COBE [60], and the Soviet Relitk, satellites [61]. The WMAP satellite also highlights that significant variability exists in the point sources and in the galactic foreground. Relative to the Universe, the findings imply isotropy over large scales, not anisotropy. All of the cosmological constants which are presented by the WMAP team are devoid of true meaning, precisely because the images are so unreliable. Given the tremendous dynamic range problems, the inability to remove the galactic foreground, the possibility of generating galactic ghosts through "cleaning", the lack of signal to noise, the lack of reproducibility, the use of coefficients which fluctuate on a yearly basis, and the problem of monitoring results on a cosmological timescale, attempts to determine cosmological constants from such data fall well outside the bounds of proper image interpretation.

In closing, it may well be appropriate to reflect once again on the words of Max Planck [63]:

> "The world is teeming with problems. Wherever man looks, some new problems crops up to meet his eye — in his home life as well as in his business or professional activity, in the realm of economics as well as in the field of technology, in the arts as well as in science. And some problems are very stubborn; they just refuse to let us in peace. Our agonizing thinking of them may sometimes reach such a pitch that our thoughts haunt us throughout the day, and even rob us of sleep at night. And if by lucky chance we succeed in solving a problem, we experience a sense of deliverance, and rejoice over the enrichment of our knowledge. But it is an entirely different story, and an experience annoying as can be, to find after a long time spent in toil and effort, that the problem which has been preying on one's mind is totally incapable of any solution at all."

**Acknowledgements**

The author would like to thank The Ohio State University for ongoing support. Luc Robitaille was responsible for the retrieval and preparation of all figures for the manuscript. The assistance of Professor Robert W. Curley is acknowledged for sample preparation and NMR acquisition required in Figure 3. The members of the Center for Advanced Biomedical Imaging associated with the design and construction of the 8 Tesla UHFMRI system [40–41] are acknowledged for enabling the acquisition and processing of the images displayed in Figures 6, 8, 9, 10, and 11.

*First published online on November 01, 2006*
*Corrections posted online on December 30, 2006*

**References**

1. WMAP website, http://map.gsfc.nasa.gov/.
2. Seife C. Breakthrough of the year: illuminating the dark Universe. *Science*, 2003, v. 302, 2038–2039.
3. Bennett C.L., Bay M., Halpern M., Hinshaw G., Jackson C., Jarosik N., Kogut A., Limon M., Meyer S.S., Page L., Spergel D.N., Tucker G.S., Wilkinson D.T., Wollack E., Wright E.L. The Microwave Anisotropy Probe mission. *Astrophys. J.*, 2003, v. 583(1), 1–23.
4. Jarosik N., Bennett C.L., Halpern M., Hinshaw G., Kogut A., Limon M., Meyer S.S., Page L., Pospieszalski M., Spergel D.N., Tucker G.S., Wilkinson D.T., Wollack E., Wright E.L., Zhang Z. Design, implementation and testing of the MAP radiometers. *Astrophys. J. Suppl. Ser.*, 2003, v. 145(2), 413–436.
5. Page L., Jackson C., Barnes C., Bennett C.L., Halpern M., Hinshaw G., Jarosik N., Kogut A., Limon M., Meyer S.S., Spergel D.N., Tucker G.S., Wilkinson D.T., Wollack E., Wright E.L. The optical design and characterization of the

Wilkinson Microwave Anisotropy Probe. *Astrophys. J.*, 2003, v. 585(1), 566–586.

6. Barnes C., Limon M., Page L., Bennett C.L., Bradley S., Halpern M., Hinshaw G., Jarosik N., Jones W., Kogut A., Meyer S., Motrunich O., Tucker G., Wilkinson D., Wollack E. The MAP satellite feed horns. *Astrophys. J. Suppl. Ser.*, 2002, v. 143(2), 567–576.
7. Bennett C.L., Halpern M., Hinshaw G., Jarosik N., Kogut A., Limon M., Meyer S.S., Page L., Spergel D.N., Tucker G.S., Wollack E., Wright E.L., Barnes C., Greason M.R., Hill R.S., Komatsu E, Nolta M.R., Odegard N., Peiris H.V., Verde L, Weiland J.L. First-year Wilkinson Microwave Anisotropy Probe (WMAP) observations: preliminary maps and basic results. *Astrophys. J. Suppl. Ser.*, 2003, v. 148(1), 1–27.
8. Hinshaw G., Barnes C., Bennett C.L., Greason M.R., Halpern M., Hill R.S., Jarosik N., Kogut A., Limon M., Meyer S.S., Odegard N., Page L., Spergel D.N., Tucker G.S., Weiland J.L., Wollack E., Wright E.L. First year Wilkinson Microwave Anisotropy Probe (WMAP) observations: data processing methods and systematic error limits. *Astrophys. J. Suppl. Ser.*, 2003, v. 148(1), 63–95.
9. Jarosik N., Barnes C., Bennett C.L, Halpern M., Hinshaw G., Kogut A., Limon M., Meyer S.S., Page L., Spergel D.N., Tucker G.S., Weiland J.L., Wollack E., Wright E.L. First year Wilkinson Microwave Anisotropy Probe (WMAP) observations: on-orbit radiometer characterization. *Astrophys. J. Suppl. Ser.*, 2003, v. 148(1), 29–37.
10. Page L., Barnes C., Hinshaw G., Spergel D.N., Weiland J.L., Wollack E., Bennett C.L., Halpern M., Jarosik N., Kogut A., Limon M., Meyer S.S., Tucker G.S., Wright E.L. First year Wilkinson Microwave Anisotropy Probe (WMAP) observations: beam profiles and window functions. *Astrophys. J. Suppl. Ser.*, 2003, v. 148(1), 39–50.
11. Barnes C., Hill R.S., Hinshaw G., Page L., Bennett C.L., Halpern M., Jarosik N., Kogut A., Limon M., Meyer S.S., Tucker G.S., Wollack E., Wright E.L. First year Wilkinson Microwave Anisotropy Probe (WMAP) observations: galactic signal contamination from sidelobe pickup. *Astrophys. J. Suppl. Ser.*, 2003, v. 148(1), 51–62.
12. Bennett C.L., Hill R.S., Hinshaw G., Nolta M.R., Odegard N., Page L., Spergel D.N., Weiland J.L., Wright E.L., Halpern M., Jarosik N., Kogut A., Limon M., Meyer S.S., Tucker G.S., Wollack E. First year Wilkinson Microwave Anisotropy Probe (WMAP) observations: foreground emission. *Astrophys. J. Suppl. Ser.*, 2003, v. 148(1), 97–117.
13. Hinshaw G., Spergel D.N, Verde L., Hill R.S, Meyer S.S, Barnes C., Bennett C.L., Halpern M., Jarosik N., Kogut A., Komatsu E., Limon M., Page L., Tucker G.S., Weiland J.L., Wollack E., Wright E.L. First year Wilkinson Microwave Anisotropy Probe (WMAP) observations: the angular power spectrum. *Astrophys. J. Suppl. Ser.*, 2003, v. 148(1), 135–159.
14. Kogut A., Spergel D.N., Barnes C., Bennett C.L., Halpern M., Hinshaw G., Jarosik N., Limon M., Meyer S.S., Page L., Tucker G.S., Wollack E., Wright E.L. First year Wilkinson Microwave Anisotropy Probe (WMAP) observations: temperature-polarization correlation. *Astrophys. J. Suppl. Ser.*, 2003, v. 148(1), 161–173.
15. Spergel D.N., Verde L., Peiris H.V., Komatsu E., Nolta M.R., Bennett C.L., Halpern M., Hinshaw G., Jarosik N., Kogut A., Limon M., Meyer S.S., Page L., Tucker G.S., Weiland J.L., Wollack E., Wright E.L. First year Wilkinson Microwave Anisotropy Probe (WMAP) observations: determination of cosmological parameters. *Astrophys. J. Suppl. Ser.*, 2003, v. 148, 175–194.
16. Verde L., Peiris H.V., Spergel D.N., Nolta M.R., Bennett C.L., Halpern M., Hinshaw G., Jarosik N., Kogut A., Limon M., Meyer S.S., Page L., Tucker G.S., Wollack E., Wright E.L. First year Wilkinson Microwave Anisotropy Probe (WMAP) observations: parameter estimation methodology. *Astrophys. J. Suppl. Ser.*, 2003, v. 148(1), 195–211.
17. Peiris H.V., Komatsu E., Verde L., Spergel D.N., Bennett C.L., Halpern M., Hinshaw G., Jarosik N., Kogut A., Limon M., Meyer S.S., Page L., Tucker G.S., Wollack E., Wright E.L. First year Wilkinson Microwave Anisotropy Probe (WMAP) observations: implications for inflation. *Astrophys. J. Suppl. Ser.*, 2003, v. 148(1), 213–231.
18. Page L., Nolta M.R., Barnes C., Bennett C.L., Halpern M., Hinshaw G., Jarosik N., Kogut A., Limon M., Meyer S.S., Peiris H.V., Spergel D.N., Tucker G.S., Wollack E., Wright E.L. First year Wilkinson Microwave Anisotropy Probe (WMAP) observations: interpretation of the TT and TE angular power spectrum peaks. *Astrophys. J. Suppl. Ser.*, 2003, v. 148(1), 233–241.
19. Komatsu E., Kogut A., Nolta M.R., Bennett C.L., Halpern M., Hinshaw G., Jarosik N., Limon M., Meyer S.S., Page L., Spergel D.N., Tucker G.S., Verde L., Wollack E., Wright E.L. First year Wilkinson Microwave Anisotropy Probe (WMAP) observations: tests of Gaussianity. *Astrophys. J. Suppl. Ser.*, 2003, v. 148(1), 119–134.
20. Barnes C., Bennett C.L., Greason M.R., Halpern M., Hill R.S., Hinshaw G., Jarosik N., Kogut A., Komatsu E., Landsman D., Limon M., Meyer S.S., Nolta M.R., Odegard N., Page L., Peiris H.V., Spergel D.N., Tucker G.S., Verde L., Weiland J.L., Wollack E., Wright E.L. First year Wilkinson Microwave Anisotropy Probe (WMAP) observations: explanatory supplement. http://lambda.gsfc.nasa.gov/product/map/pub_papers/firstyear/supplement/WMAP_supplement.pdf
21. Nolta M.R., Wright E.L., Page L., Bennett C.L., Halpern M., Hinshaw G., Jarosik N., Kogut A., Limon M., Meyer S.S., Spergel D.N., Tucker G.S., Wollack E. First year Wilkinson Microwave Anisotropy Probe observations: dark energy induced correlation with radio sources. *Astrophys. J.*, 2004, v. 608(1), 10–15.
22. Jarosik N., Barnes C., Greason M.R., Hill R.S., Nolta M.R, Odegard N., Weiland J.L., Bean R., Bennett C.L., Dore O., Halpern M., Hinshaw G., Kogut A., Komatsu E., Limon M., Meyer S.S., Page L., Spergel D.N., Tucker G.S., Wollack E., Wright E.L. Three-year Wilkinson Microwave Anisotropy Probe (WMAP) observations: beam profiles, data processing, radiometer characterization and systematic error limits. *Astrophys. J.*, 2006, *submitted*.
23. Hinshaw G., Nolta M.R., Bennett C.L., Bean R., Dore O., Greason M.R., Halpern M., Hill R.S., Jarosik N., Kogut A., Komatsu E., Limon M., Odegard N., Meyer S.S., Page L.,

Peiris H.V., Spergel D.N., Tucker G.S., Verde L., Weiland J.L., Wollack E., Wright E.L. Three-year Wilkinson Microwave Anisotropy Probe (WMAP) observations: temperature analysis. *Astrophys. J.*, 2006, *submitted*.

24. Page L., Hinshaw G., Komatsu E., Nolta M.R., Spergel D.N., Bennett C.L., Barnes C., Bean R., Dore O., Halpern M., Hill R.S., Jarosik N., Kogut A., Limon M., Meyer S.S., Odegard N., Peiris H.V., Tucker G.S., Verde L., Weiland J.L., Wollack E., Wright E.L. Three-year Wilkinson Microwave Anisotropy Probe (WMAP) observations: polarization analysis. *Astrophys. J.*, 2006, *submitted*.
25. Spergel D.N., Bean R., Dore O., Nolta M.R., Bennett C.L., Hinshaw G., Jarosik N., Komatsu E., Page L., Peiris H.V., Verde L., Barnes C., Halpern M., Hill R.S., Kogut A., Limon M., Meyer S.S., Odegard N., Tucker G.S., Weiland J.L., Wollack E., Wright E.L. Three-year Wilkinson Microwave Anisotropy Probe (WMAP) observations: implications for cosmology. *Astrophys. J.*, 2006, *submitted*.
26. Barnes C., Bean R., Bennett C.L., Dore O., Greason M.R., Halpern M., Hill R.S., Hinshaw G., Jarosik N., Kogut A., Komatsu E., Landsman D., Limon M., Meyer S.S., Nolta M.R., Odegard N., Page L., Peiris H.V., Spergel D.N., Tucker G.S., Verde L., Weiland J.L., Wollack E., Wright E.L. Three-year Wilkinson Microwave Anisotropy Probe (WMAP) observations: three year explanatory supplement. http://map.gsfc.nasa.gov/m_mm/pub_papers/supplement/wmap_3yr_supplement.pdf
27. NASA, new satellite data on Universe's first trillionth second. WMAP Press Release. http://map.gsfc.nasa.gov/m_or/PressRelease_03_06.html.
28. In-cites. "Super hot" papers in science published since 2003. http://www.in-cites.com/hotpapers/shp/1-50.html.
29. Tegmark M., de Oliveira-Costa A., Hamilton A.J.S. A high resolution foreground cleaned CMB map from WMAP. *Phys. Rev. D*, 2003, v. 68(12), 123523.
30. Robitaille P.M.L., Scott R.D., Wang J., Metzler D.E. Schiff bases and geminal diamines derived from pyridoxal 5'-phosphate and diamines. *J. Am. Chem. Soc.*, 1989, v. 111, 3034–3040.
31. Robyt J.F., White B.J. Biochemical techniques: theory and practice. Brooks/Cole Publishing Company, Monterey, CA, 1987, p. 261–262.
32. Schaefer J. Selective saturation of Carbon-13 lines in Carbon-13 Fourier transform NMR experiments. *J. Magn. Reson.*, 1972, v. 6, 670–671.
33. Plateau P., Guerron M. Exchangeable proton NMR without baseline distortion, using new strong pulse sequences. *J. Am. Chem. Soc.*, 1982, v. 104, 7310–7311.
34. Redfield A.G, Kunz S.D., Ralph E.K. Dynamic range in Fourier transform proton magnetic resonance. *J. Magn. Reson.*, 1975, v. 19, 114–117.
35. Sklenar V., Starcuk Z. 1-2-1 pulse train: a new effective method of selective excitation for proton NMR in water. *J. Magn. Reson.*, 1983, v. 54, 146–148.
36. Turner D.L. Binomial solvent suppression. *J. Magn. Reson.*, 1983, v. 54, 146–148.
37. Hurd R.E. Gradient enhanced spectroscopy. *J. Magn. Reson.*, 1990, v. 87(2), 422–428.
38. Moonen C.T.W., van Zijl P.C.M. Highly effective water suppression for in-vivo proton NMR-spectroscopy (DRYSTEAM). *J. Magn. Reson.*, 1990, v. 88(1), 28–41.
39. Cavanagh J., Fairbrother J.W., Palmer III A.G., Skelton N.J. Protein NMR spectroscopy: principles and practice. Academic Press, New York, 1995.
40. Robitaille P.M.L., Abduljalil A.M., Kangarlu A., Zhang X., Yu Y., Burgess R., Bair S., Noa P., Yang L., Zhu H., Palmer B., Jiang Z., Chakeres D.M., Spigos D. Human magnetic resonance imaging at eight Tesla. *NMR Biomed.*, 1998, v. 11, 263–265.
41. Robitaille P.M.L., Abduljalil A.M., Kangarlu A. Ultra high resolution imaging of the human head at 8 Tesla: 2K × 2K for Y2K. *J Comp. Assist. Tomogr.*, 2000, v. 24, 2–7.
42. Robitaille P.M.L., Berliner L.J. (eds). Biological magnetic resonance: ultra high field magnetic resonance imaging. Springer, New York, 2006.
43. Liang Z.P., Lauterbur P.C. Principles of magnetic resonance imaging: a signal processing perspective. IEEE Press, New York, 2000.
44. Belliveau J.W., Kennedy Jr. D.N., McKinstry R.C., Buchbinder B.R., Weisskoff R.M., Cohen M.S., Vevea J.M., Brady T.J., Rosen B.R. Functional mapping of the human visual cortex by magnetic resonance imaging. *Science*, 1991, v. 254(5032), 716–9.
45. Ogawa S., Tank D.W., Menon R., Ellermann J.M., Kim S.G., Merkle H., Ugurbil K. Intrinsic signal changes accompanying sensory stimulation: functional brain mapping with magnetic resonance imaging. *Proc. Natl. Acad. Sci. USA*, 1992, v. 89(13), 5951–5.
46. Bandettini P.A., Jesmanowicz A., Wong E.C., Hyde J.S. Processing strategies for time-course data sets in functional MRI of the human brain. *Magn. Reson. Med.*, 1993, v. 30(2), 161–73.
47. Gaskell C.M., Klimek E.S. Variability of active galactic nuclei from the optical to X-Ray regions. *Astronom. Astrophysic. Trans.*, 2003, v. 22(4–5), 661–679.
48. COBE web site, http://lambda.gsfc.nasa.gov/product/cobe/.
49. Robitaille P.M.L. NMR and the age of the Universe. *American Physical Society Centenial Meeting*, BC19.14, March 21, 1999.
50. Kirchhoff G. Ueber das Verhaltnis zwischen dem Emissionsvermogen und dem absorptionsvermogen der Körper für Waeme und Litcht. *Annalen der Physik*, 1860, v. 109, 275–301.
51. Planck M. The theory of heat radiation. Philadelphia, PA., P. Blakiston's Son, 1914.
52. Robitaille P.M.L. On the validity of Kirchhoff's law of thermal emission. *IEEE Trans. Plasma Sci.*, 2003, v. 31(6), 1263–1267.
53. Robitaille P.M.L. An analysis of universality in blackbody radiation. *Progr. in Phys.*, 2006, v. 2, 22–23.
54. Planck M. Ueber das Gesetz der energieverteilung in Normalspectrum. *Annalen der Physik*, 1901, v. 4, 553–563.

55. Stefan J. Ueber die Beziehung zwischen der Wärmestrahlung und der Temperature. *Sitzungsberichte der mathematischnaturwissenschaftlichen Classe der kaiserlichen Akademie der Wissenschaften*, Wien 1879, v. 79, 391–428.

56. Wien W. Ueber die Energieverteilung in Emissionspektrum eines schwarzen Körpers. *Ann. Phys.*, 1896, v. 58, 662–669.

57. Robitaille P.M.L. The MAP satellite: a powerful lesson in thermal physics. *Spring Meeting of the American Physical Society Northwest Section*, F4.004, May 26, 2001.

58. Robitaille P.M.L. The collapse of the Big Bang and the gaseous Sun. *New York Times*, March 17, 2002.

59. Robitaille P.M.L. WMAP: an alternative explanation for the dipole. *Fall Meeting of the American Physical Society Ohio Section*, E2.0001, 2006.

60. Fixsen D.L., Gheng E.S., Gales J.M., Mather J.C., Shafer R.A., Wright E.L. The Cosmic Microwave Background spectrum from the full COBE FIRAS data set. *Astrophys. J.*, 1996, v. 473, 576–587.

61. Klypin A.A, Strukov I.A., Skulachev D.P. The Relikt missions: results and prospects for detection of the Microwave Background Anisotropy. *Mon. Not. Astr. Soc.*, 1992, v. 258, 71–81.

62. Robitaille P.M.L. On the origins of the CMB: insight from the COBE, WMAP and Relikt-1 satellites. *Progr. in Phys.*, 2007, v. 1, 19–23.

63. Planck M. Scientific autobiography. Philosophical Library, New York, 1949.